

# Lawrence Berkeley National Laboratory

## LBL Publications

### Title

Passivation and Degradation of Sulfur-Treated Silicon Surfaces for Photovoltaics

### Permalink

<https://escholarship.org/uc/item/29n7w117>

### Journal

The Journal of Physical Chemistry C, 129(7)

### ISSN

1932-7447

### Authors

Hua, Amandee  
Upadhyaya, Ajay  
Mouri, Tasnim K  
[et al.](#)

### Publication Date

2025-02-20

### DOI

10.1021/acs.jpcc.4c07457

### Copyright Information

This work is made available under the terms of a Creative Commons Attribution-NoDerivatives License, available at <https://creativecommons.org/licenses/by-nd/4.0/>

Peer reviewed

## **Passivation and Degradation of Sulfur-Treated Silicon Surfaces for Photovoltaics**

*Amandee Hua<sup>1\*</sup>, Ajay Upadhyaya<sup>2</sup>, Tasnim K. Mouri<sup>3</sup>, Isaac Lam<sup>3</sup>, Wanli Yang<sup>4</sup>, Ajeet Rohatgi<sup>2</sup>, Ujjwal K. Das<sup>3</sup>, Dirk Hauschild<sup>1,5</sup>, Lothar Weinhardt<sup>1,5</sup>, Clemens Heske<sup>1,5&</sup>*

<sup>1</sup> Department of Chemistry and Biochemistry, University of Nevada, Las Vegas (UNLV),  
4505 Maryland Parkway, Las Vegas, NV 89154-4003, USA

<sup>2</sup> School of Electrical and Computer Engineering, Georgia Institute of Technology, North  
Avenue, Atlanta, GA 30332, USA

<sup>3</sup> Institute of Energy Conversion, University of Delaware, 451 Wyoming Road, Newark, DE  
19716, USA

<sup>4</sup> Advanced Light Source, Lawrence Berkeley National Laboratory, 1 Cyclotron Rd, Berkeley,  
CA 94720, USA

<sup>5</sup> Institute for Photon Science and Synchrotron Radiation (IPS) and Institute for Chemical  
Technology and Polymer Chemistry (ITCP), Karlsruhe Institute of Technology (KIT),  
Kaiserstr. 12, 76131 Karlsruhe, Germany

Keywords: x-ray photoelectron spectroscopy, x-ray emission spectroscopy, chemical  
structure, sulfur passivation, silicon solar cells

& heske@unlv.nevada.edu

## Abstract

Sulfur-based passivation for silicon surfaces using H<sub>2</sub>S gas is an alternative passivation method to reduce the thermal budget for Si photovoltaics. To understand the impact of the high-quality passivation and an observed passivation efficiency decrease after air exposure, we have studied the chemical surface structure by x-ray photoelectron spectroscopy (XPS), x-ray Auger electron spectroscopy (XAES), and S and Si L<sub>2,3</sub> x-ray emission spectroscopy (XES). On the S-passivated silicon surfaces, we find the formation of S-Si bonds, in addition to some Si-O bonds. Upon air exposure, sulfur partially desorbs from the Si surface and an increased presence of Si-O and S-O bonds is observed. We identify that well-defined S-Si bonds are crucial to maintain high-quality surface passivation for Si photovoltaics, which allows further optimization of the fabrication process for S-based passivation on silicon.

## 1. Introduction

Among the existing photovoltaic materials, including CdTe, Cu(In,Ga)Se<sub>2</sub>, GaAs, perovskites, and many more<sup>1</sup>, silicon continues to dominate the global market<sup>2</sup>, reaching record efficiencies above 26%<sup>3</sup> for submodules (274 cm<sup>2</sup>) and above 24%<sup>4</sup> on large areas (17,806 cm<sup>2</sup>). Over the past decades, the development of various Si surface passivation techniques has played an important role in the advancement of Si photovoltaics. Clean crystalline Si surfaces inherently have dangling bonds, which provide recombination centers for photogenerated electron-hole pairs<sup>5</sup>, hence lowering the overall efficiency<sup>6,7</sup>. In addition, a high defect density can pin the Fermi level<sup>5</sup>, potentially forming unfavorable band alignments. Thus, removing such dangling bonds via surface passivation is crucial for high-efficient solar cells. Many types of passivation techniques are implemented by either eliminating the dangling bonds (chemical passivation) and/or decreasing the recombination probability (field-effect passivation)<sup>8-10</sup>. One of the most common passivation layers for Si photovoltaics is SiO<sub>2</sub>. However, high quality SiO<sub>2</sub> passivation through thermal oxidation requires a processing temperature above 850 °C.<sup>11,12</sup> Such high temperatures increase the thermal budget, making Si photovoltaics more expensive, and potentially lower the bulk quality of silicon. These unfavorable qualities encourage the exploration of low-temperature passivation techniques, such as the use of Ga<sub>2</sub>O<sub>3</sub><sup>13</sup>, graphene oxide<sup>14</sup>, and many more<sup>15</sup>. From theoretical calculations, sulfur is also identified as a candidate to passivate the dangling bonds at the Si surface<sup>16,17</sup>. Additionally, experimental studies using low-energy electron diffraction (LEED) showed sulfur to restore reconstructed Si surfaces to bulk-terminated surface structures.<sup>18-20</sup> Recently, we used H<sub>2</sub>S gas to passivate the Si surface for photovoltaics. In this method, a lower processing temperature of 550 °C was applied as compared to other studies.<sup>21-24</sup> Here, an effective minority carrier lifetime  $\tau_{\text{eff}} > 2000 \mu\text{s}$ , which is comparable to thermal oxide passivation, and a ~20% efficiency passivated emitter and rear contact (PERC) solar cell could be achieved.<sup>22,23</sup> However, a significant decrease in the passivation quality, as determined by an increase in surface recombination velocity (SRV), is observed with prolonged air exposure.<sup>21</sup> Thus, studying the impact of the S-passivation of the silicon surface on the chemical structure, as well as the role of subsequent air exposure, is crucial to further improve this passivation approach.

In this paper, the chemical structures of three sample sets of crystalline Si(100) wafer surfaces are analyzed with varying doping type and concentration. For this purpose, the samples were studied after S-passivation and after air exposure for ~8 days using a unique combination of spectroscopic techniques, namely x-ray photoelectron spectroscopy (XPS), x-ray Auger electron spectroscopy (XAES), and soft x-ray emission spectroscopy (XES).

## 2. Experimental

Three sets of silicon wafers from the University of Delaware and the Georgia Institute of Technology were studied in this work. Two of the sample sets consisted of n-type Si wafers with doping concentrations of  $2.3$  and  $1.5 \times 10^{15} \text{ cm}^{-3}$  (in the following referred to as “n1” and “n2”, respectively). The Si wafers in the third set were p-type, with a doping concentration of  $7.0 \times 10^{15} \text{ cm}^{-3}$  (“p” in the following). Each sample set was composed of an “untreated”, “passivated”, and “degraded” Si wafer. The “untreated” samples were cleaned with an HF/HNO<sub>3</sub> acid mixture, a sulfuric acid and hydrogen peroxide (SPM) mixture, and a final HF etch, with deionized water rinsing in-between each step. The S-passivation was performed in a chemical vapor deposition (CVD) reactor, pumped down below  $10^{-6}$  Torr, and using an H<sub>2</sub>S/Ar gas mixture at  $550 \text{ }^\circ\text{C}$  for 30 minutes. The H<sub>2</sub>S gas had a purity of 99.9% with CO<sub>2</sub>, H<sub>2</sub>O, and hydrocarbons contributing as the main impurities. A detailed description of the cleaning and passivation process is presented in references <sup>21-23</sup>. Subsequently, the S-passivated Si wafers were degraded through air exposure for  $\sim 8$  days at 40% relative humidity in a desiccator. Effective minority carrier lifetimes  $\tau_{\text{eff}}$  were measured for each Si wafer after passivation and degradation at the University of Delaware using a Sinton WCT-100 tool<sup>25</sup>. For the n1 Si wafers,  $\tau_{\text{eff}} > 2000$  and  $\sim 6 \text{ } \mu\text{S}$  were measured after passivation and degradation, respectively. For the n2 Si wafers,  $\tau_{\text{eff}}$  was  $> 1000 \text{ } \mu\text{S}$  after passivation, and decreased to  $\sim 5 \text{ } \mu\text{S}$  after degradation. Lastly, for the p Si wafers, an  $\tau_{\text{eff}}$  of  $> 150 \text{ } \mu\text{S}$  was measured after passivation, which decreased to  $\sim 3 \text{ } \mu\text{S}$  with exposure to air.

For surface characterization, sister samples were processed, immediately vacuum-sealed in a glovebox, and then shipped to the University of Nevada, Las Vegas (UNLV) for XPS and XAES measurements. At UNLV, the samples were inserted via a nitrogen-filled glovebox into the ultra-high vacuum system without further air exposure. Measurements were performed with a SPECS XR 50 Mg K <sub>$\alpha$</sub>  and Al K <sub>$\alpha$</sub>  twin anode x-ray source and a SPECS PHOIBOS 150 1D-DLD electron analyzer. The analyzer was calibrated according to references <sup>26,27</sup>. For calibration at kinetic energies corresponding to the Si KLL Auger lines, the Au 4f<sub>7/2</sub> photoemission peak (excited using Al K <sub>$\alpha$</sub> ) of a Au sample biased with 220 V bias voltage was measured as well. After the XPS and XAES measurements, the samples were re-sealed in a nitrogen-filled bag (without exposure to air) and shipped to Beamline 8.0.1 at the Advanced Light Source (ALS), Lawrence Berkeley National Lab (LBNL) for XES measurements using the iRIXS<sup>28</sup> and our SALSA<sup>29</sup> endstations. While the SiS<sub>2</sub> reference spectrum was measured at the iRIXS endstation, all other spectra were measured at the SALSA endstation. The S and Si L<sub>2,3</sub> emission energy axis was calibrated using prominent spectral features in the S L<sub>2,3</sub> XES of CdS<sup>30</sup> and the elastic line (in higher order) of a C K RIXS (Resonant Inelastic X-ray Scattering) map, in addition to a C K XAS (X-ray Absorption Spectroscopy) spectrum of HOPG<sup>31</sup>, respectively, unless otherwise stated.

### 3. Results and discussion

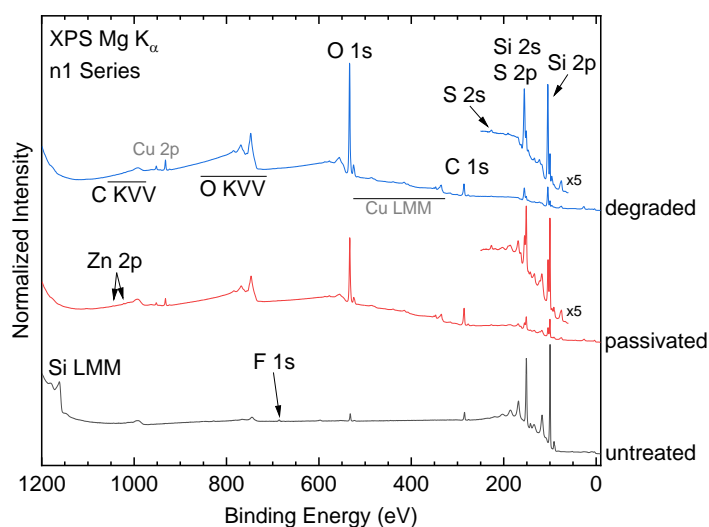


**Figure 1.** XPS Mg  $K_{\alpha}$  survey spectra of the untreated (black), passivated (red), and degraded (blue) silicon wafers of the n1 series. All spectra shown are normalized to the total spectral area. For the “passivated” and “degraded” spectra, the regions between 250 and 60 eV are also shown after multiplication by a factor of 5. Prominent photoemission and Auger peaks are labeled.<sup>27</sup>

Figure 1 shows the XPS survey spectra of the n1 series for the untreated, passivated, and degraded Si surfaces, while the n2 and p series are shown in the supplemental information (Figure S1). The spectrum of the untreated sample is dominated by Si peaks, as expected, with some minor carbon and oxygen signals that can be attributed to surface adsorbates. In addition, a small amount of residual fluorine is also visible, likely due to the use of HF in the cleaning process.<sup>32</sup> Upon passivation, small sulfur-related peaks are observed (and will be discussed below). The Si peaks are reduced (most notably the Si 2p), while oxygen and carbon signals significantly increase in intensity. This highlights the inherent (and practically probably unavoidable) presence of oxygen in this specific sulfur passivation process. Possible sources are the  $H_2S$  gas (99.9% purity) or adsorbates from the chamber wall desorbing during the temperature ramp-up in the passivation process. To test this latter hypothesis, the silicon wafer was also heated to 600 °C (i.e., beyond the standard 550 °C) and in *argon* atmosphere in the same chamber, also yielding a significant amount of oxygen (and fluorine) on the surface (see Figure S2). Moreover, minor zinc and copper signals are detected. The former is a common trace metal found in silicon<sup>33,34</sup>, while the latter could be due to the use of adhesive copper tape for the sample mounting process. For the degraded sample, i.e., after exposure to air for 8 days, the oxygen signal further increases, while the sulfur peaks decrease slightly in intensity.

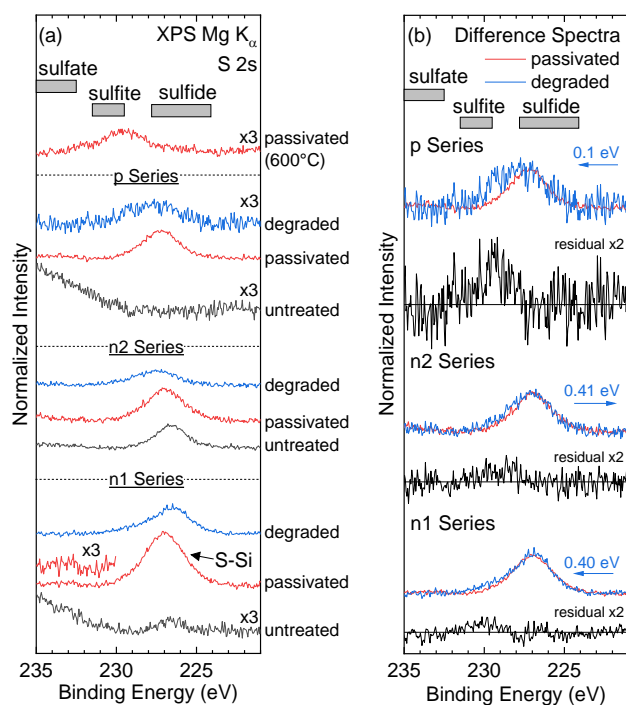


**Figure 2.** (a) XPS Mg K $\alpha$  S 2s spectra of all silicon wafers (n1, n2, and p series). All spectra are normalized to the area of the Si 2p area (see Figure 3a). Also, an n1 Si wafer from a separate sample set is shown after S-passivation at 600 °C (topmost spectrum, see text for details). (b) Direct comparison of the S 2s spectra of the passivated (red) and degraded (blue) Si wafers. All spectra were normalized to peak maximum intensity; to better compare changes in the lineshape, the degraded spectra were shifted by the amounts indicated by the blue arrows to align with the spectra of the passivated samples. Afterwards, differences between the degraded and passivated spectra were computed to analyze the spectral changes. Difference spectra (residuals) are shown in black, multiplied by a factor of 2. A linear background is subtracted from all spectra shown in Figures 2a) and 2b). Gray bars represent literature-based binding energies of different sulfur chemical environments.<sup>27</sup>

To obtain a detailed picture of the impact of the passivation and degradation steps, the local chemical environment of sulfur and silicon are investigated in the following. Figure 2a shows the S 2s regions of the various silicon wafers. The n1 and n2 untreated silicon wafers show the presence of sulfur, likely from the use of the SPM mixture during the cleaning process.<sup>32,35</sup> No sulfur signal is found for the untreated sample of the *p series*. In contrast, the more bulk-sensitive (and background-free) S L<sub>2,3</sub> XES spectra reveal the presence of sulfur in *all* samples (Figures 4 and 5).

After S-passivation, a S 2s XPS peak is found at ~227 eV for all three series. We assign this to a sulfide-like chemical environment, i.e., to the formation of S-Si bonds, which is later confirmed by S L<sub>2,3</sub> XES measurements. In addition to the peak at ~227 eV, a small peak at ~232 eV is visible in the n1 series (as seen when magnified by a factor of 3), indicating a small degree of S-O bonds. Comparing with reference binding energies, this is likely a highly oxidized (e.g., sulfate-like) chemical environment. We surmise that the sulfur impurities found in the untreated Si wafer, and/or unreacted sulfur remaining from the H<sub>2</sub>S passivation, subsequently oxidize during the S-passivation process. Alternatively, some of the S atoms (from the S-Si bonds) may oxidize, forming S-O bonds.

For all Si wafers, the S 2s intensities decrease by ~50 % and broaden *after degradation*, suggesting a loss of sulfur at the surface and a change in chemical bonding. To analyze the peak broadening in Figure 2 b), the S 2s spectra were normalized to their peak maxima, the degraded (blue) spectra were slightly shifted to align their low-binding energy side with the spectra of the passivated samples, and difference spectra (i.e., “degraded – passivated” residuals) were calculated. The shift indicates a change in surface band-bending and/or a difference in the local chemical environment. All three difference spectra (magnified by a factor of two) show intensity at ~229.5 eV. This binding energy is ascribed to the formation of S-O bonds with intermediate oxidation state, such as that found for a sulfite chemical environment. This assignment is further supported by comparing with the position of the sulfur peak (at ~229.5 eV) of the n1 Si wafer that was S-passivated at 600 °C (Figure 2a, topmost spectrum). Due to a higher temperature, an increased presence of oxygen is found (see Figure S2). Thus, after exposure to air, the sulfur content at the surface decreases and an additional S-O bonding environment is observed, while some S-Si bonds remain unaffected.

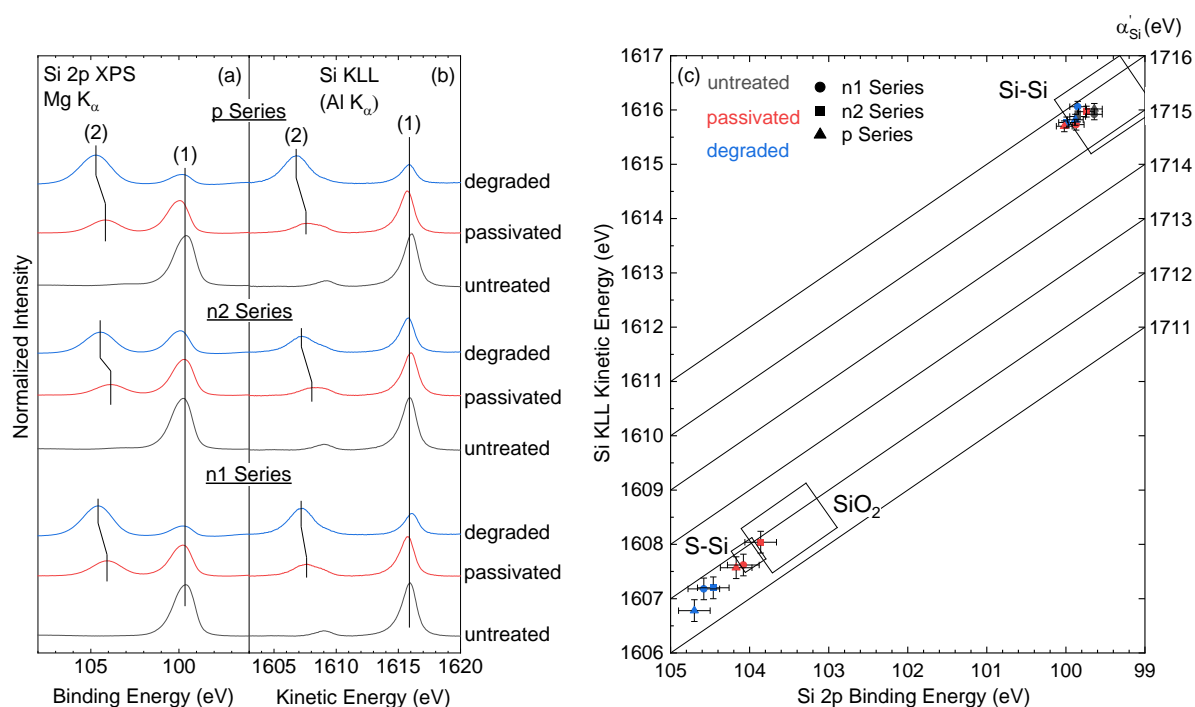


**Figure 3.** (a) Si 2p XPS and (b) Si KLL Auger spectra of the investigated silicon wafer surfaces. The spectra are normalized to the corresponding Si 2p and Si KLL areas. (c) Wagner plot displaying the Si 2p binding energy on the abscissa, the kinetic energy of the prominent Si KLL peak on the ordinate, and the modified Auger Parameter on the diagonal lines. For each sample, two data points were calculated using the positions of the features labeled (1) and (2), respectively. The two boxed areas mark reference values<sup>27,36</sup> typically found for SiO<sub>2</sub> and (pure) Si-Si chemical environments, while the region labeled “S-Si” represents data points observed in this paper. The colors indicate the different treatments, while the shapes represent the sample series of the Si wafers.

Figures 3a and 3b show the Si 2p and KLL spectra, respectively. All untreated samples exhibit one major peak, marked (1), at ~100 and ~1616 eV in the Si 2p and Si KLL data, respectively. After passivation, this main peak decreases in intensity. Additionally, peaks emerge at ~104 eV in the Si 2p and ~1607.5 eV in the Si KLL data (marked with (2)). While, for the passivated samples, peaks (2) are smaller than peaks (1), the situation is reversed for the degraded samples.

To further analyze the Si chemical environments, the Si 2p binding energies,  $E_{\text{Bind}}(\text{Si } 2p)$ , the Si KLL kinetic energies,  $E_{\text{Kin}}(\text{Si KLL})$ , and the modified Auger parameters  $\alpha'_{\text{Si}} = E_{\text{Kin}}(\text{Si KLL}) + E_{\text{Bind}}(\text{Si } 2p)$  are shown in a Wagner plot in Figure 3c. The modified Auger parameter has the advantage of being insensitive to band bending changes and charging, and thus purely depends on the chemical environment.<sup>37</sup> Boxes are labeled indicating reference value ranges<sup>27,36</sup> for pure Si and SiO<sub>2</sub>. For the studied samples, the  $E_{\text{Bind}}(\text{Si } 2p)$  of the peaks labeled (1) and (2) were combined with the  $E_{\text{Kin}}(\text{Si KLL})$  of the peaks with the same numbers and are shown as colored symbols in Figure 3c. The data points computed from peaks (1) appear in the top-right corner of Figure 3c, with an average  $\alpha'_{\text{Si}} = 1517.8 \pm 0.2$  eV, which can be assigned to Si in a pure Si environment. Note how all  $\alpha'_{\text{Si}}$  are essentially identical within the error bar, indicating the same chemical environment. The small observed variations in  $E_{\text{Bind}}(\text{Si } 2p)$  and  $E_{\text{Kin}}(\text{Si KLL})$  can thus most likely be attributed to changes in band bending, which could be influenced by impurities and bulk characteristics such as doping concentration and type. The data points computed from peaks (2) appear in the bottom-left region of the Wager plot, with an average  $\alpha'_{\text{Si}} = 1607.4 \pm 0.6$  eV, and are labeled as “S-Si”. This value is similar to the range found for SiO<sub>2</sub>, while the XPS and XAES energies differ. SiS<sub>2</sub> and SiO<sub>2</sub> have been reported to show very similar energies,<sup>36,38</sup> which makes an unambiguous determination by XPS and XAES alone very difficult. In the following, we will thus use XES for a more direct probe of these chemical environments.

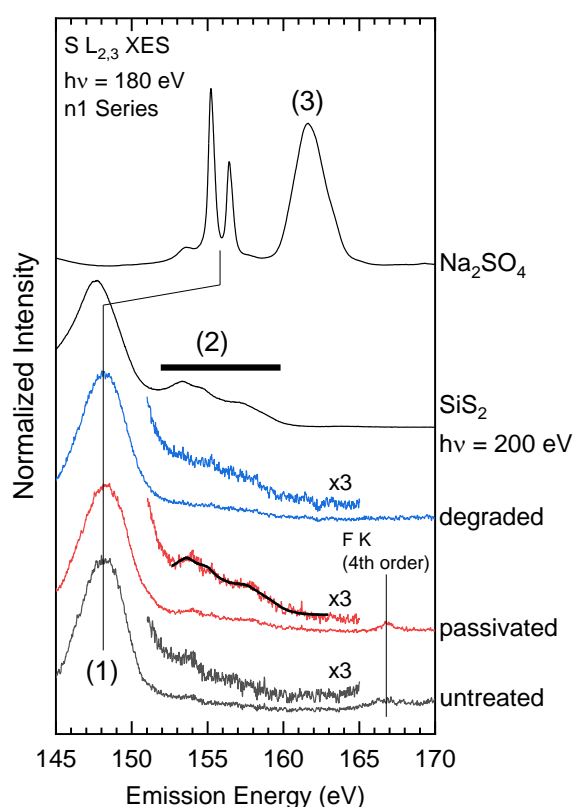


**Figure 4.** S L<sub>2,3</sub> XES ( $h\nu_{\text{exc.}} = 180$  eV) of the silicon wafers of the n1 series. Reference spectra of SiS<sub>2</sub> and Na<sub>2</sub>SO<sub>4</sub> are shown for comparison. The upper valence band (UVB) region (152 - 165 eV) is magnified by a factor of 3 for the Si wafer samples. To emphasize the presence of S-Si bonds, the spectrum of the passivated sample (red) is overlaid with the SiS<sub>2</sub> reference spectrum (black, shifted by 0.27 eV to higher emission energies for best agreement) in the UVB region.

The XPS and XAES data set is complemented by S L<sub>2,3</sub> (Figures 4 and 5) and Si L<sub>2,3</sub> (Figure 6) XES data. While the (more surface-sensitive) XPS and XAES spectra only vary slightly

between the n1, n2, and p series after the passivation and degradation processes, significant differences are observed in XES. The n1 series is discussed first (Figure 4) and then later compared to the other two series. To identify the spectral signatures of S-Si bonds and sulfates, Figure 4 shows the S L<sub>2,3</sub> XES spectra of SiS<sub>2</sub> and Na<sub>2</sub>SO<sub>4</sub> powder references. The spectrum of SiS<sub>2</sub> is dominated by transitions from S 3s derived bands around 148 eV (1) and weaker transitions from the upper valence band at higher energies, as marked with a black bar labeled (2). For Na<sub>2</sub>SO<sub>4</sub>, the transitions involving the S 3s derived states are shifted to higher emission energies, with peaks at 155.2 eV and 156.4 eV, and we find intensity at 161.6 eV that is attributed to S 3d derived states.<sup>39</sup> Although the S 2s XPS spectra of the n1 series in Figure 2a show a very weak sulfate-related peak for the passivated sample, no evidence of sulfates is found in the XES spectra of the n1 series Si wafers in Figure 4 due to the reduced surface sensitivity. All Si samples show a characteristic S 3s to S 2p transition at ~148 eV (1), indicative of the presence of sulfur with an oxidation state  $\leq 0$ <sup>40,41</sup>, which corroborates with the S 2s peaks found in the XPS spectra in Figure 2. To ascertain that no other Si XES lines could be the origin for the feature at ~148 eV, spectra of SiO<sub>2</sub> powder, Si<sub>3</sub>N<sub>4</sub>, SiC, and quartz were recorded in the same region and do not show a peak at ~148 eV (see Figure S3). In contrast, a different commercial silicon wafer (VWR International) also shows spectral intensity at ~148 eV, further supporting the hypothesis of a general presence of sulfur in/on nominally “untreated” Si wafers (possibly from other treatments during the manufacture).

Due to unfavorable dipole selection rules, the upper valence band (UVB) between 151 and 162 eV is rather weak in S L<sub>2,3</sub> XES spectra; it is thus also shown magnified (x3) in Figure 4. In particular, S contributes to the UVB with S 3p states, for which, strictly speaking, emission is dipole forbidden in S L<sub>2,3</sub> XES. The observed intensity in the UVB region is thus indicative for *hybridization* of the S states with covalent bonding partners (including S-S bonding). The weak intensity in the UVB region of the S L<sub>2,3</sub> XES for the Si wafers thus suggests S with only weak covalent interaction and mostly ionic character. Upon closer inspection, the weak intensity in the UVB region of the n1 series shows similarities to the SiS<sub>2</sub> reference spectrum. This is most pronounced for the passivated sample - the overlaid SiS<sub>2</sub> UVB spectrum (black) shows a very good agreement with the sample spectrum (red), indicating the formation of S-Si bonds. Note that the SiS<sub>2</sub> reference spectrum is shifted by 0.27 eV to higher emission energies for best agreement, which is likely related to the uncertainty in energy calibration between different experimental stations and beamtimes. As marked in Figure 4, some fluorine K emission (excited with higher-order light of the beamline and detected in the 4<sup>th</sup> order of the spectrometer) is found for the untreated and passivated samples, in agreement with the small F 1s signal found in XPS in Figure 1.

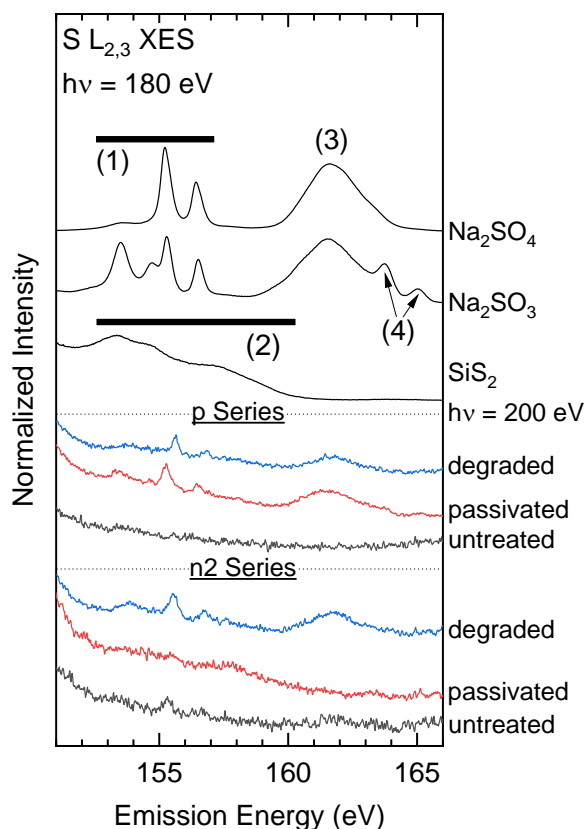


**Figure 5.** UVB region of the S L<sub>2,3</sub> XES of the n2 and p series. Sample spectra are normalized to the S 3s to S 2p transition at ~148 eV (not shown). Na<sub>2</sub>SO<sub>4</sub>, Na<sub>2</sub>SO<sub>3</sub>, and SiS<sub>2</sub> references are also shown, with prominent spectral features marked by numbers.

Figure 5 shows the UVB region of the S L<sub>2,3</sub> XES spectra of the n2 and p series in comparison with Na<sub>2</sub>SO<sub>4</sub> (sulfate), Na<sub>2</sub>SO<sub>3</sub> (sulfite), and SiS<sub>2</sub> reference spectra. The prominent spectral features are marked by numbers (1) through (4). The transitions from S 3s derived states (1) are found at 153.5 and 154.7 eV for Na<sub>2</sub>SO<sub>3</sub> and 155.2 and 156.4 eV for Na<sub>2</sub>SO<sub>4</sub>, respectively. The sulfite spectrum also contains transitions indicative of sulfate, likely caused by beam-induced formation of sulfate and/or contamination in the reference powder.<sup>42</sup> Both Na<sub>2</sub>SO<sub>4</sub> and Na<sub>2</sub>SO<sub>3</sub> show emission from S 3d derived states (3), with Na<sub>2</sub>SO<sub>3</sub> exhibiting two additionally peaks (4) at 163.8 and 165.0 eV. Comparing the reference spectra with the silicon wafer spectra, we find the following. All spectra show some weak and broad intensity between 153 and 160 eV, indicating some S-Si bonding. Furthermore, the untreated and degraded spectra of the n2 series, as well as the passivated and degraded spectra of the p series, exhibit clear signals indicative of sulfates. Variations in the peak positions between the references and sample spectra can be related to different cations.<sup>39</sup> Additionally, we find sulfite spectral features for the degraded sample of the n2 series and the passivated sample of the p series (at ~153.5 eV).

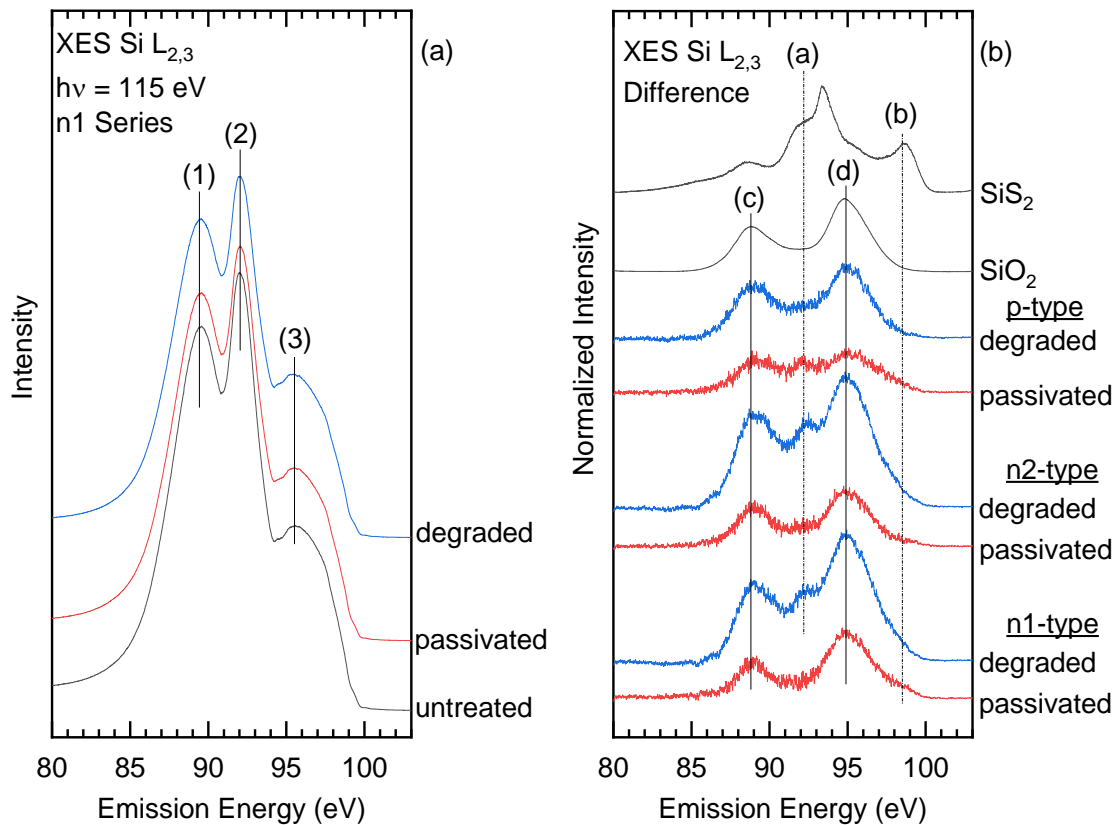


**Figure 6.** (a) Si  $L_{2,3}$  XES of the Si wafers in the n1 series. Characteristic Si  $L_{2,3}$  features are marked (1)-(3). (b) Difference of passivated and untreated spectra (red), as well as difference of degraded and untreated spectra (blue) of the respective sample series. SiO<sub>2</sub> and SiS<sub>2</sub> reference spectra are shown for comparison, with prominent features denoted by the vertical lines marked (a) - (d).

The local chemical environment of Si is discussed in the following with the XES Si  $L_{2,3}$  spectra in Figure 6. The spectra of the n1 series depicted in Figure 6a show the characteristic signature of crystalline Si, which is characterized by three intense peaks at 89.5 (1), 92.1 (2), and 95.5 eV (3).<sup>43</sup> At first sight, no significant differences are evident between the differently treated samples of the n1 series (and similarly for the n2 and p series, not shown). This is not unexpected due to the bulk-sensitivity of the XES measurements – most of the probed silicon atoms will not be affected by any kind of surface treatment. Here, the incoming and outgoing photons are attenuated by the characteristic  $1/e$  attenuation length of  $\sim 50$  nm and  $\sim 590$  nm at 115 and 90 eV, respectively.<sup>44</sup> To become sensitive to subtle (surface) changes in the Si spectra, difference spectra (Figure 6b) were calculated by subtracting a maximal amount of the “untreated” spectrum from the respective “passivated” (red) and “degraded” (blue) spectra. The spectra are normalized at 92.1 eV and shifted  $\pm 0.02$  eV prior to subtraction for optimal alignment. In Fig. 6, the spectra of SiO<sub>2</sub> and SiS<sub>2</sub> reference powders are also shown for comparison. All difference spectra resemble the SiO<sub>2</sub> reference spectrum, suggesting the formation of Si-O bonds. After degradation, the relative intensity of the remaining (oxide) spectral contribution increases. These observations are in agreement with the XPS results discussed above. Note that additional intensity is found at 92.2 eV for some of the difference spectra, i.e., close to the energy of the strongest peak in the Si  $L_{2,3}$  XES spectra; we surmise that this is an artifact from the subtraction routine. Also, the presence of another minority Si species cannot be entirely ruled out. However, no evidence for S-Si bonds is observed in the Si  $L_{2,3}$

difference spectra - the feature marked with (b) is absent. This is not surprising since, in contrast to S  $L_{2,3}$  XES that exclusively probes the environment of the *sulfur* atoms, the contribution of silicon atoms bonded to sulfur in the Si  $L_{2,3}$  XES is likely below the (relative) detection limit.

The electron and x-ray spectroscopy data discussed above now allows us to describe the passivation and degradation mechanisms, as follows. While all studied Si wafers already show small amounts of S in the untreated crystals, we find a prominent increase of sulfur at the surface after passivation and can identify S-Si bonds. Furthermore, we note an increase of  $\text{SiO}_2$  as well, possibly due to the presence of oxygen during the elevated temperature of the passivation process. After subsequent air exposure, a clear decrease in the sulfur content and an increase of the amount of  $\text{SiO}_2$  are detected. This interaction with air is likely due to moisture, forming  $\text{H}_2\text{S}$  that subsequently desorbs. This loss of sulfur passivation can be correlated with the significant decrease in minority carrier lifetime observed in the degraded samples, regardless of Si wafer type. Similarly, we find a correlation between the degrees of oxidation for the passivated samples: The largest effective minority carrier lifetime ( $>2000 \mu\text{S}$ ) is observed for the n1 passivated sample, for which the lowest degree of surface oxidation and the clearest signature of S-Si bonding is found. In contrast, the other passivation series, with shorter effective minority carrier lifetime, exhibit a higher degree of sulfur-oxygen bond formation and/or a weaker S-Si bond signature.

## Summary

The impact of a novel sulfur passivation approach and subsequent air-induced degradation on Si surfaces for photovoltaic applications is investigated using photoelectron, Auger electron, and soft x-ray emission spectroscopy, making use of the different degrees of surface sensitivity of these techniques. The spectra paint a detailed picture of the chemical changes induced by the passivation process and shed light on the degradation mechanism occurring during air exposure. The observed changes in surface chemical structure are correlated with the observed changes in effective minority carrier lifetimes after passivation and degradation. We find the sulfur passivation approach to efficiently bond sulfur to the Si wafer surface but observe a loss of sulfur as well as a Si oxide formation after air exposure. Although sulfur passivation using  $\text{H}_2\text{S}$  has the potential to be an alternative low-temperature passivation technique for Si surfaces, the preservation of a well-defined S-Si bond environment (especially after air exposure) is crucial to maintain high-quality surface passivation for Si photovoltaics.

## Acknowledgements

This work was supported by US Department of Energy's Office of Energy Efficiency and Renewable Energy (EERE) under the Solar Energy Technologies Office (SETO) Agreement DE-EE0008554. This research used resources from the Advanced Light Source, which is a U.S. Department of Energy (DOE) Office of Science User Facility under Contract No. DE-AC02-05CH11231. We gratefully acknowledge the support of Nan Jiang (UNLV) and Robert Theisen (University of Delaware) in the preparation of samples and execution of experimental campaigns.

Received: ((will be filled in by the editorial staff))

Revised: ((will be filled in by the editorial staff))

Published online: ((will be filled in by the editorial staff))

## References

- (1) Fazal, M. A.; Rubaiee, S. Progress of PV Cell Technology: Feasibility of Building Materials, Cost, Performance, and Stability. *Solar Energy* **2023**, *258*, 203–219. <https://doi.org/10.1016/j.solener.2023.04.066>.
- (2) Fraunhofer Institute for Solar Energy Systems, ISE. *Photovoltaics Report, 2022*. <https://www.ise.fraunhofer.de/content/dam/ise/de/documents/publications/studies/Photovoltaics-Report.pdf> (accessed 2022-05-09).
- (3) Lin, H.; Yang, M.; Ru, X.; Wang, G.; Yin, S.; Peng, F.; Hong, C.; Qu, M.; Lu, J.; Fang, L.; Han, C.; Procel, P.; Isabella, O.; Gao, P.; Li, Z.; Xu, X. Silicon Heterojunction Solar Cells with up to 26.81% Efficiency Achieved by Electrically Optimized Nanocrystalline-Silicon Hole Contact Layers. *Nat Energy* **2023**, *8* (8), 789–799. <https://doi.org/10.1038/s41560-023-01255-2>.
- (4) Green, M. A.; Dunlop, E. D.; Yoshita, M.; Kopidakis, N.; Bothe, K.; Siefert, G.; Hao, X. Solar Cell Efficiency Tables (Version 62). *Progress in Photovoltaics* **2023**, *31* (7), 651–663. <https://doi.org/10.1002/pip.3726>.
- (5) Tao, M. Removal of Surface States on Si(1 0 0) by Valence-Mending Passivation. *Applied Surface Science* **2018**, *462*, 8–17. <https://doi.org/10.1016/j.apsusc.2018.08.049>.
- (6) Fonash, S. J. *Solar Cell Device Physics*, 2nd ed.; Academic Press/Elsevier: Burlington, MA, 2010.
- (7) *Handbook of Surfaces and Interfaces of Materials*; Nalwa, H. S., Ed.; Academic Press: San Diego, 2001.
- (8) Bonilla, R. S.; Wilshaw, P. R. A Technique for Field Effect Surface Passivation for Silicon Solar Cells. *Appl. Phys. Lett.* **2014**, *104* (23), 232903. <https://doi.org/10.1063/1.4882161>.
- (9) Aberle, A. G. Surface Passivation of Crystalline Silicon Solar Cells: A Review. *Prog. Photovolt: Res. Appl.* **2000**, *8* (5), 473–487. [https://doi.org/10.1002/1099-159X\(200009/10\)8:5<473::AID-PIP337>3.0.CO;2-D](https://doi.org/10.1002/1099-159X(200009/10)8:5<473::AID-PIP337>3.0.CO;2-D).
- (10) Balaji, N.; Hussain, S. Q.; Park, C.; Raja, J.; Yi, J.; Jeyakumar, R. Surface Passivation Schemes for High-Efficiency c-Si Solar Cells - A Review. *Transactions on Electrical and Electronic Materials* **2015**, *16* (5), 227–233. <https://doi.org/10.4313/TEEM.2015.16.5.227>.
- (11) Aberle, A. G.; Glunz, S. W.; Stephens, A. W.; Green, M. A. High-Efficiency Silicon Solar Cells: Si/SiO<sub>2</sub>, Interface Parameters and Their Impact on Device Performance. *Prog. Photovolt: Res. Appl.* **1994**, *2* (4), 265–273. <https://doi.org/10.1002/pip.4670020402>.
- (12) Benick, J.; Zimmermann, K.; Spiegelman, J.; Hermle, M.; Glunz, S. W. Rear Side Passivation of PERC-Type Solar Cells by Wet Oxides Grown from Purified Steam: Rear Side Passivation of PERC-Type Solar Cells. *Prog. Photovolt: Res. Appl.* **2011**, *19* (3), 361–365. <https://doi.org/10.1002/pip.1020>.
- (13) Allen, T. G.; Cuevas, A. Plasma Enhanced Atomic Layer Deposition of Gallium Oxide on Crystalline Silicon: Demonstration of Surface Passivation and Negative Interfacial Charge. *Physica Rapid Research Ltrs* **2015**, *9* (4), 220–224. <https://doi.org/10.1002/pssr.201510056>.
- (14) Vaqueiro-Contreras, M.; Bartlam, C.; Bonilla, R. S.; Markevich, V. P.; Halsall, M. P.; Vijayaraghavan, A.; Peaker, A. R. Graphene Oxide Films for Field Effect Surface Passivation of Silicon for Solar Cells. *Solar Energy Materials and Solar Cells* **2018**, *187*, 189–193. <https://doi.org/10.1016/j.solmat.2018.08.002>.
- (15) Grant, N. E.; Murphy, J. D. Temporary Surface Passivation for Characterisation of Bulk Defects in Silicon: A Review. *Physica Rapid Research Ltrs* **2017**, *11* (11), 1700243. <https://doi.org/10.1002/pssr.201700243>.

- (16) Krüger, P.; Pollmann, J. *Ab Initio* Calculations of Si, As, S, Se, and Cl Adsorption on Si(001) Surfaces. *Phys. Rev. B* **1993**, *47* (4), 1898–1910. <https://doi.org/10.1103/PhysRevB.47.1898>.
- (17) Kaxiras, E. Semiconductor-Surface Restoration by Valence-Mending Adsorbates: Application to Si(100):S and Si(100):Se. *Phys. Rev. B* **1991**, *43* (8), 6824–6827. <https://doi.org/10.1103/PhysRevB.43.6824>.
- (18) Lacharme, J. P.; Benazzi, N.; Sébenne, C. A. Compositional and Electronic Properties of Si(001)2×1 upon Diatomic Sulfur Interaction. *Surface Science* **1999**, *433–435*, 415–419. [https://doi.org/10.1016/S0039-6028\(99\)00450-1](https://doi.org/10.1016/S0039-6028(99)00450-1).
- (19) Papageorgopoulos, A. Deposition of Sulfur on Si(100)2×1: Surface Restoration. *Solid State Communications* **1997**, *101* (5), 383–387. [https://doi.org/10.1016/S0038-1098\(96\)00603-5](https://doi.org/10.1016/S0038-1098(96)00603-5).
- (20) Metzner, H.; Hahn, Th.; Bremer, J.-H. Structure of Sulphur-Terminated Silicon Surfaces. *Surface Science* **1997**, *377–379*, 71–74. [https://doi.org/10.1016/S0039-6028\(96\)01356-8](https://doi.org/10.1016/S0039-6028(96)01356-8).
- (21) Das, U. K.; Theisen, R.; Hua, A.; Upadhyaya, A.; Lam, I.; Mouri, T. K.; Jiang, N.; Hauschild, D.; Weinhardt, L.; Yang, W.; Rohatgi, A.; Heske, C. Efficient Passivation of n-type and p-type Silicon Surface Defects by Hydrogen Sulfide Gas Reaction. *J. Phys.: Condens. Matter* **2021**, *33* (46), 464002. <https://doi.org/10.1088/1361-648X/ac1ec8>.
- (22) Das, U.; Theisen, R.; Hanket, G.; Upadhyaya, A.; Rohatgi, A.; Hua, A.; Weinhardt, L.; Hauschild, D.; Heske, C. Sulfurization as a Promising Surface Passivation Approach for Both n- and p-type Si. In *2020 47th IEEE Photovoltaic Specialists Conference (PVSC)*; IEEE: Calgary, AB, Canada, 2020; pp 1167–1170. <https://doi.org/10.1109/PVSC45281.2020.9300395>.
- (23) Mouri, T. K.; Upadhyaya, A.; Rohatgi, A.; Ok, Y.-W.; Upadhyaya, V.; Rounsaville, B.; Hua, A.; Hauschild, D.; Weinhardt, L.; Heske, C.; Das, U. K. Hydrogen Sulfide Passivation for P-Type Passivated Emitter and Rear Contact Solar Cells. *IEEE J. Photovoltaics* **2024**, *14* (2), 211–218. <https://doi.org/10.1109/JPHOTOV.2023.3338095>.
- (24) Liu, H.-Y.; Das, U. K.; Birkmire, R. W. Surface Defect Passivation and Reaction of C-Si in H<sub>2</sub>S. *Langmuir* **2017**, *33* (51), 14580–14585. <https://doi.org/10.1021/acs.langmuir.7b03520>.
- (25) Sinton, R. A.; Cuevas, A. Contactless Determination of Current–Voltage Characteristics and Minority-Carrier Lifetimes in Semiconductors from Quasi-Steady-State Photoconductance Data. *Applied Physics Letters* **1996**, *69* (17), 2510–2512. <https://doi.org/10.1063/1.117723>.
- (26) Seah, M. P. Post-1989 Calibration Energies for X-Ray Photoelectron Spectrometers and the 1990 Josephson Constant. *Surf. Interface Anal.* **1989**, *14* (8), 488–488. <https://doi.org/10.1002/sia.740140813>.
- (27) Moulder, J. F.; Stickle, W. F.; Sobol, P. E.; Bomben, K. D. *Handbook of X-Ray Photoelectron Spectroscopy*; Perkin-Elmer Corporation Physical Electronics Division, 1992.
- (28) Qiao, R.; Li, Q.; Zhuo, Z.; Sallis, S.; Fuchs, O.; Blum, M.; Weinhardt, L.; Heske, C.; Pepper, J.; Jones, M.; Brown, A.; Spucce, A.; Chow, K.; Smith, B.; Glans, P.-A.; Chen, Y.; Yan, S.; Pan, F.; Piper, L. F. J.; Denlinger, J.; Guo, J.; Hussain, Z.; Chuang, Y.-D.; Yang, W. High-Efficiency *in Situ* Resonant Inelastic X-Ray Scattering (iRIXS) Endstation at the Advanced Light Source. *Review of Scientific Instruments* **2017**, *88* (3), 033106. <https://doi.org/10.1063/1.4977592>.
- (29) Blum, M.; Weinhardt, L.; Fuchs, O.; Bär, M.; Zhang, Y.; Weigand, M.; Krause, S.; Pookpanratana, S.; Hofmann, T.; Yang, W.; Denlinger, J. D.; Umbach, E.; Heske, C. Solid and Liquid Spectroscopic Analysis (SALSA)—a Soft X-Ray Spectroscopy

- Endstation with a Novel Flow-through Liquid Cell. *Review of Scientific Instruments* **2009**, *80* (12), 123102. <https://doi.org/10.1063/1.3257926>.
- (30) Weinhardt, L.; Fuchs, O.; Fleszar, A.; Bär, M.; Blum, M.; Weigand, M.; Denlinger, J. D.; Yang, W.; Hanke, W.; Umbach, E.; Heske, C. Resonant Inelastic Soft X-Ray Scattering of CdS: A Two-Dimensional Electronic Structure Map Approach. *Phys. Rev. B* **2009**, *79* (16), 165305. <https://doi.org/10.1103/PhysRevB.79.165305>.
- (31) Watts, B.; Ade, H. A Simple Method for Determining Linear Polarization and Energy Calibration of Focused Soft X-Ray Beams. *Journal of Electron Spectroscopy and Related Phenomena* **2008**, *162* (2), 49–55. <https://doi.org/10.1016/j.elspec.2007.08.008>.
- (32) Verhaverbeke, S.; Messoussi, R.; Morinaga, H.; Ohmi, T. Recent Advances in Wet Processing Technology and Science. *MRS Proc.* **1995**, *386*, 3. <https://doi.org/10.1557/PROC-386-3>.
- (33) Kern, W. Overview and Evolution of Silicon Wafer Cleaning Technology. In *Handbook of Silicon Wafer Cleaning Technology*; Elsevier, 2018; pp 3–85. <https://doi.org/10.1016/B978-0-323-51084-4.00001-0>.
- (34) Allardyce, G.; Barr, R.; Chan, R.; Moynihan, M.; O'Connor, C.; Ridler, T. Interaction between Post Wire Saw Cleaning and the Subsequent Cell Fabrication Saw Damage Etch and Texturing Process. In *2010 35th IEEE Photovoltaic Specialists Conference*; IEEE: Honolulu, HI, USA, 2010; pp 003494–003497. <https://doi.org/10.1109/PVSC.2010.5614741>.
- (35) Zazzera, L. C.; Becker, L. S. Investigation of H<sub>2</sub>SO<sub>4</sub>:H<sub>2</sub>O<sub>2</sub>, Dilute HF and DI Water Silicon Wafer Cleaning Processes. In *Semiconductor Cleaning Technology*; The Electrochemical Society, Incorporated: Hollywood, Florida, USA, 1989; Vol. 90–9, pp 43–58.
- (36) NIST X-ray Photoelectron Spectroscopy Database. *NIST Standard Reference Database Number 20*. National Institute of Standards and Technology, Gaithersburg MD, 20899. doi:10.18434/T4T88K (accessed 2022-07-31).
- (37) Moretti, G. Auger Parameter and Wagner Plot in the Characterization of Chemical States by X-ray Photoelectron Spectroscopy: A Review. *Journal of Electron Spectroscopy and Related Phenomena* **1998**, *95* (2–3), 95–144. [https://doi.org/10.1016/S0368-2048\(98\)00249-7](https://doi.org/10.1016/S0368-2048(98)00249-7).
- (38) Morgan, W. E.; Van Wazer, J. R. Binding Energy Shifts in the X-Ray Photoelectron Spectra of a Series of Related Group IVa Compounds. *J. Phys. Chem.* **1973**, *77* (7), 964–969. <https://doi.org/10.1021/j100626a023>.
- (39) Weinhardt, L.; Hauschild, D.; Steininger, R.; Jiang, N.; Blum, M.; Yang, W.; Heske, C. Sulfate Speciation Analysis Using Soft X-Ray Emission Spectroscopy. *Anal. Chem.* **2021**, *93* (23), 8300–8308. <https://doi.org/10.1021/acs.analchem.1c01187>.
- (40) Heske, C.; Groh, U.; Fuchs, O.; Umbach, E.; Franco, N.; Bostedt, C.; Terminello, L. J.; Perera, R. C. C.; Hallmeier, K. H.; Preobrajenski, A.; Szargan, R.; Zweigart, S.; Riedl, W.; Karg, F. X-Ray Emission Spectroscopy of Cu(In,Ga)(S,Se)<sub>2</sub>-Based Thin Film Solar Cells: Electronic Structure, Surface Oxidation, and Buried Interfaces. *phys. stat. sol. (a)* **2001**, *187* (1), 13–24. [https://doi.org/10.1002/1521-396X\(200109\)187:1<13::AID-PSSA13>3.0.CO;2-D](https://doi.org/10.1002/1521-396X(200109)187:1<13::AID-PSSA13>3.0.CO;2-D).
- (41) Meisel, A.; Steuer, I.; Szargan, R. Das Röntgen-L<sub>2,3</sub>-Emissionsspektrum Des Schwefels in Verschiedenen Verbindungen. *Spectrochimica Acta* **1967**, *23B*, 527–533.
- (42) Duncan, D. A.; Kephart, J. M.; Horsley, K.; Blum, M.; Mezher, M.; Weinhardt, L.; Häming, M.; Wilks, R. G.; Hofmann, T.; Yang, W.; Bär, M.; Sampath, W. S.; Heske, C. Characterization of Sulfur Bonding in CdS:O Buffer Layers for CdTe-Based Thin-Film Solar Cells. *ACS Appl. Mater. Interfaces* **2015**, *7* (30), 16382–16386. <https://doi.org/10.1021/acsami.5b03503>.

- (43) Rubensson, J.-E.; Mueller, D.; Shuker, R.; Ederer, D. L.; Zhang, C. H.; Jia, J.; Callcott, T. A. Excitation-Energy Dependence in the  $L_{2,3}$  Fluorescence Spectrum of Si. *Phys. Rev. Lett.* **1990**, *64* (9), 1047–1050. <https://doi.org/10.1103/PhysRevLett.64.1047>.
- (44) Henke, B. L.; Gullikson, E. M.; Davis, J. C. X-Ray Interactions: Photoabsorption, Scattering, Transmission, and Reflection at  $E=50\text{-}30000$  eV,  $Z=1\text{-}92$ , Atomic Data and Nuclear Data Tables. **1993**, *54* (2), 181–342.